Title
3-D In-Bi-Sn Electrodes for Lab-on-PCB Cell Sorting

Journal
IEEE Transactions on Components Packaging and Manufacturing Technology, 6(9)

ISSN
2156-3950

Authors
Luo, Jason
Simon, Melinda G
Jiang, Alan YL
et al.

Publication Date
2016-09-01

DOI
10.1109/tcpmt.2016.2573161

Peer reviewed

3-D In-Bi-Sn Electrodes for Lab-on-PCB Cell Sorting

Jason Luo, Melinda G. Simon, Alan Y. L. Jiang, Edward L. Nelson, Abraham P. Lee, Guann-Pyng Li, and Mark Bachman

***Abstract*— We present a microfluidic lab-on-printed circuit board (PCB) device containing alloy vertical electrodes for sorting microparticles using dielectrophoresis. The device consists of a hydrodynamic prefocuser and an electronic sorting region. Lining the two sidewalls of the electronic sorting region are regularly spaced rectangular metal electrodes reaching from the floor to the ceiling of the flow channel that bridge electric field lines laterally across the channel. The size and distribution of these vertical electrodes are arranged asymmetrically such that the resultant electric field forms sharp electric field gradients across the channel; specific geometries were optimized using finite element methods. Particles entering the device are initially focused on a single stream as they pass through the prefocuser. Subsequently, they are exposed to the lateral electric field gradient and separate into streams based on their size and dielectric properties. Validation was performed by dielectrophoretically separating live cells from dead cells. Importantly, the system presented can be readily integrated with various external sensors and actuators using commercially available components owing to the device's integration into a PCB.**

***Index Terms*— Dielectrophoresis (DEP), microelectrode, microfluidic.**

I. Introduction

OVER the past 15 years, microfluidic devices have gained popularity as a tool for the miniaturization of a wide variety of biological and biomedical assays. The applications of microfluidics are myriad, spanning fields such as healthcare, biodefense, and environmental monitoring, but are all based on providing the researcher or clinician with methods for manipulating fluids by taking advantage of characteristics exclusive to submilliliter scales, namely, the relative dominance of surface tension and laminar flow over the effects of gravity and turbulence. Ultimately, the goal is to transfer complicated and labor-intensive laboratory processes into a handheld chip, thus saving time, labor, and wet bench consumables. Current microfluidic methods for label-free particle and cell separation, an important unit operation in many biological assays, include inertial focusing, deterministic lateral displacement, and dielectrophoresis (DEP). Each of these methods exploits certain features of fluidic operations on the microscale to enable the separation, such as the use of high flow rates that enable focusing of small particles in defined streams (inertial focusing), the use of microfabricated structures on the same size scale of the cells or particles (deterministic lateral displacement), or the use of a nonhomogeneous electric field that can impart a significant force to cells or particles at the microscale (DEP) [1]. Microfluidic cell and particle separations have been applied to many fields of biological and chemical research including cancer cell isolation for diagnostics [2] and stem cell characterization and enrichment [3], [4]. DEP is arguably among the most mature of these microfluidic label-free cell separation techniques, having been applied to separations involving cancer cells from blood as early as the 1990s [5], [6] and more recently in the enrichment of stem and progenitor cell populations in preparation for transplantation studies [4], [7].

A. 3-D Electrodes

Many DEP devices consist of polymer microchannels aligned over planar interdigitated electrodes patterned on the device substrate. When attached to an external power supply and a function generator, the electrodes project electric field lines into the microchannel. The electric field lines are thus densest at the edges of the electrodes and sparsest away from them, forming an electric field gradient. However, these devices share some common shortcomings. In general, very sharp gradients exist near the planar electrodes, but rapidly dissipate away from them. Particles thus experience different dielectrophoretic forces depending on their randomized vertical starting positions in the channel cross section: those nearest the electrodes will experience a strong DEP force, while the rest may slip through the device unsorted by passing through a region of particularly low gradient, e.g., near the channel ceiling, away from the electrodes. Second, many DEP devices with an interdigitated electrode configuration separate cells or particles in batches [4], [7], [8] rather than one by one in a continuous manner, limiting the throughput of such approaches

Manuscript received January 19, 2016; revised April 21, 2016; accepted May 15, 2016. Date of publication August 12, 2016; date of current version September 20, 2016. This work was supported in part by the National Science Foundation through the IGERT Program under Grant 0549479 and in part by the National Cancer Institute within the National Institutes of Health under Grant P30CA062203. The work of the author M. G. Simon was supported in part by the California Institute of Regenerative Medicine under Grant TG201152 and in part by the ARCS Foundation, Orange County chapter. Recommended for publication by Associate Editor R. Mahajan upon evaluation of reviewers' comments. *(Jason Luo and Melinda G. Simon contributed equally to this work.)*

J. Luo, A. Y. L. Jiang, and A. P. Lee are with the Department of Biomedical Engineering, University of California at Irvine, Irvine, CA 92697 USA (e-mail: jtluo@uci.edu; yljiang@uci.edu; aplee@uci.edu).

M. G. Simon was with the University of California at Irvine, Irvine, CA 92697 USA. She is now with the Lawrence Livermore National Laboratory, Livermore, CA 94550 USA (e-mail: simon27@lllnl.gov).

E. L. Nelson is with the Department of Medicine, Institute for Immunology, University of California at Irvine, Irvine, CA 92697 USA (e-mail: enelson@uci.edu).

G. P. Li and M. Bachman are with the Department of Electrical Engineering and Computer Science, University of California at Irvine, Irvine, CA 92697 USA (e-mail: gpli@uci.edu; mbachman@uci.edu).

Color versions of one or more of the figures in this paper are available online at http://ieeexplore.ieee.org.

Digital Object Identifier 10.1109/TCPMT.2016.2573161

and increasing the need for automation and controls to execute various steps of the separation process [4], [9].

Vertical electrodes are a potential solution to overcome these issues. In contrast to their planar predecessors, vertical electrodes are 3-D solid or liquid structures cast into the walls of a microfluidic channel using various microfabrication techniques. Positioned on either side of the microfluidic channel, and spanning its entire height, these 3-D electrodes project vertically uniform electric fields into the microchannel. Along the horizontal plane, the shape and steepness of the gradient are controlled by adjusting the size and positions of the electrodes and of any insulating features in the channel that might further distort the field lines [10]. Alternatively, vertical electrodes of the same geometry on either side of a channel can be fabricated with dielectrophoretic steering forces provided by actuation of electrodes on either side of the channel with different frequencies or voltages [11], [12].

Despite the advantages of vertical electrode use for DEP separations, the fabrication can be challenging, generally requiring a series of photolithographic steps [13] and, in the case of electroplating, fine electrical current control to fabricate these 3-D structures and then to seal the device [10]. Various methods have been proposed to circumvent these difficulties such as contactless DEP and insulator-based DEP [14]. These methods have been successful at performing DEP separations, but often require high-electric fields, which can be dangerous to operate and add to the cost of the system [15], [16].

A novel method is presented for combining the convenience of liquid electrode fabrication with the durability and performance of their metal counterparts. In addition, our method allows for out-of-cleanroom fabrication of these vertical electrodes, thus significantly decreasing the time and cost required for their fabrication. Using a low-melting-point indium-based solder and exploiting the increased importance of surface tension forces at the microscale, 3-D electrodes can be rapidly and reliably formed in 5 min using only a hotplate [17].

B. Lab-on-PCB

To further increase the accessibility and applicability of the technology, we mount our device on a printed circuit board (PCB) platform, which provides connection from an external power source to the microelectrodes. The use of a PCB for this purpose provides several benefits, chief among them is the use of a standard and mature technology for the preparation of conductive traces. Indeed, there have been efforts to design PCB accompaniments to microfluidic devices [9], [18], but work to integrate PCB functionality directly into the microfluidic device has been very limited [19].

The development of microfluidic devices on PCBs also makes the device amenable to the integration of ancillary components for signal generation, amplification, other electronic components, and miniaturized pumps and valves. PCBs offer an avenue to solve a common problem in the development of microfluidic systems, which routinely require several pieces of bulky lab equipment, and the integration of these components onto the PCB would truly realize the vision of a fully integrated platform (commonly termed as a lab-on-a-chip system). Such an integrated platform would undoubtedly increase the interest and adoption of these systems within the laboratories of the envisioned end-users of the technology—clinicians and biological researchers, owing to the complete automation they would offer. Finally, PCBs offer a final advantage of scalability, and are readily mass-produced in contrast to glass microfluidic chips containing traces comprised of thin metal films, which must be etched in small batches.

To demonstrate the utility of these approaches, a PCB-based microfluidic device was prepared for sorting particles using DEP, a mechanism that has found widespread use in the microfluidics community. This PCB enabled a facile and robust connection of the solder electrodes to external prototyping wires used to deliver the electrical actuation signal.

II. Theory of Dielectrophoresis-Based Sorting

A full description of the DEP theory is beyond the scope of this paper; instead, a short description is offered here with the interested reader directed to several recent reviews [20], [21]. Briefly, when exposed to an electric field, dielectric particles polarize to form induced dipoles. In a nonuniform dc electric field, the pole closer to the field maxima experiences an electrostatic force stronger than that felt by the end closer to the field minima, resulting in a net translational force in the direction of the field maxima. If the field is generated using an ac signal, the direction of the force is not as straightforward, and the particle's polarizability relative to that of the medium becomes a factor. If the particle is more polarizable than the medium, it will indeed travel up the field gradient, and if the particle is less polarizable than the medium, it will travel down that same gradient. These two effects are termed as positive DEP (pDEP) and negative DEP, respectively.

For homogeneous spherical particles in a homogeneous medium, the time-averaged DEP force is modeled as

$$\vec{F}_{\mathrm{DEP}} = 2\pi r^3 \varepsilon_m \mathrm{Re(CM)} \vec{\nabla} |\vec{E}|^2 \tag{1}$$

where r is the particle radius, ε_m is the relative permittivity of the media, Re(CM) is the real component of the Clausius–Mossotti relation, and $\vec{\nabla}|\vec{E}|^2$ is the gradient of the square of the electric field. The Clausius–Mossotti relation, which takes into consideration the relative polarizabilities of the particles and the medium, is expressed as the following:

$$\frac{\varepsilon_p^* - \varepsilon_m^*}{\varepsilon_p^* + 2\varepsilon_m^*} \tag{2}$$

where

$$\varepsilon_i^* = \varepsilon_0 \varepsilon_r - i\frac{\sigma}{\omega} \tag{3}$$

with σ = electrical conductivity of the material and $\omega = 2\pi f$ is the angular frequency.

From (2), the real component of the Clausius–Mossotti factor ranges from $-(1/2)$ for spherical particles infinitely less polarizable than the medium to $+1$ for the opposite extreme [22].

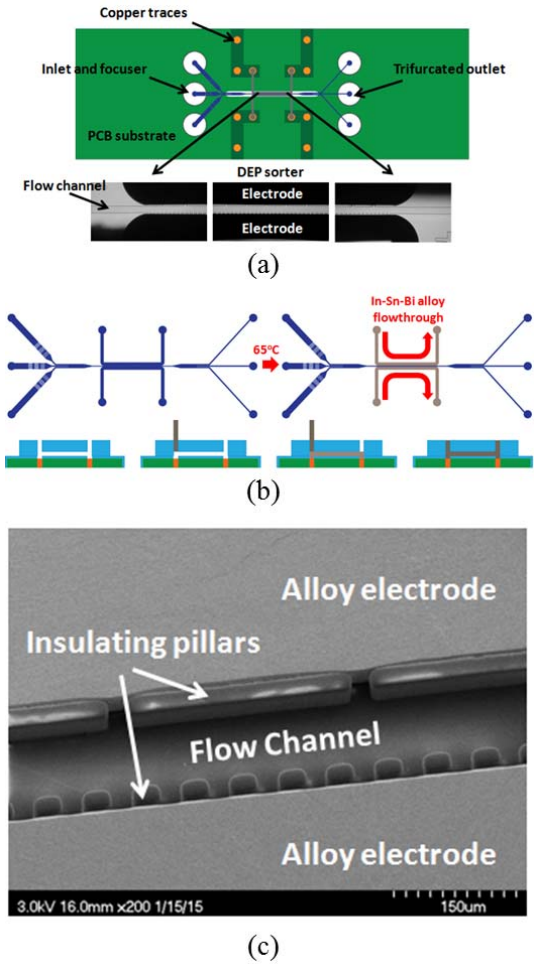

Fig. 1. (a) Device schematic, to scale. The device consists of a hydrodynamic flow prefocuser that directs all incoming particles into a single line, and an electronic component that injects an electric field gradient into the channel and sorts the stream of particles based on their size and dielectric properties. (b) Electrodes are formed by flowing alloy into side channels (shown in gray) parallel to the main channel (shown in blue). Gaps in the walls between the main channel and the side channels expose the electrodes to the main channel. (c) Particle suspension is hydrodynamically focused into a thin stream to ensure that all particles experience identical DEP conditions as they pass through the electronic sorter.

Finally, acting against the DEP force is the drag force governed by Stokes's law; particles reach terminal velocity when these two forces balance, as expressed in

$$v = \frac{\vec{F}_{\mathrm{DEP}}}{6\pi\eta r} = \frac{2\pi r^2 \varepsilon_m \mathrm{Re}(\mathrm{CM})\vec{\nabla}|\vec{E}|^2}{6\pi\eta r} \tag{4}$$

where η is the viscosity of the suspending medium.

Thus, DEP separation of particles in a mixed suspension functions primarily due to different net forces experienced by different particles, owing to the particles' size and dielectric properties. Because these variations depend on the particles' size and polarizability, as well as the geometry and frequency of the electric field gradient applied, DEP has widely used in recent years to detect and sort microscale particles, from polystyrene beads to rare mammalian cells based on subtle differences between their physical and electronic properties.

III. Materials and Methods

A. Device Fabrication

The presented device consists of an inlet, a hydrodynamic prefocuser, an electronic sorter, and three outlets for recovering sorted particles (Fig. 1). Device channels were first cast in polydimethylsiloxane (PDMS) (Ellsworth Adhesives, Germantown, WI) from a silicon wafer master, patterned using deep reactive ion etching (DRIE). Once the DRIE master has been fabricated, all other steps of the fabrication, including vertical electrode fabrication, can be completed outside of the cleanroom environment. The electronic sorting component consists of two side channels, each parallel to the main channel and separated from it by a line of evenly spaced pickets. At each end, the main channel branches into three inlets/outlets. In Fig. 1(a), the inlet trifurcation serves as an injection point for the particle suspension and the focusing buffer, while the outlet trifurcation allows the user to divide the sorted particles into three batches for recovery.

To facilitate electrical and fluidic connections to the device, a $1'' \times 3''$ printed circuit board containing all necessary electrical leads and fluidic ports was designed in EagleCAD (CadSoft Computer, Ft. Lauderdale, FL, USA) and custom printed (Smart-Prototyping, Kowloon, HK). A bespoke protocol was used to bond the PDMS channels to the PCB. Briefly, a layer of PDMS approximately 5-mm thick was applied to the surface of the PCB, providing a smooth surface to facilitate a strong bond between the board and the PDMS film, preventing delamination. Subsequently, the PDMS slab containing the patterned microchannels was covalently sealed channel-side-down against the PDMS film using plasma treatment.

To form the vertical electrodes themselves, devices were placed on a hotplate, heated to 90 °C, and a low-melting point alloy of 51% indium, 32.5% bismuth, and 16.5% tin (Indium Corporation, Clinton, NY) was gently flowed into the side channels using hydraulic pressure through vias in the PCB aligned over the inlets and outlets of the side channels. The alloy's high-viscosity forces it to flow laminarly through the side channels, while the high-surface tension owing to the small radius of curvature between pickets prevents the solder from entering the main fluidic channel [Fig. 1(b)] [17]. After the alloy was in place, the device was cooled and the alloy solidified. To make a connection to external electronics, wires were soldered to the vias on the back side of the PCB.

Finally, the device is connected to an external amplifier and function generator [Fig. 1(b)]. Fluid flow is driven using two syringe pumps (Harvard Apparatus, Holliston, MA, USA). Visualization is performed using inverted fluorescent microscopy (Olympus Corp., Tokyo, JP) and digital imaging (Nikon Corp., Tokyo, JP). Videos were recorded using a commercial SLR camera (Canon 5D Mark II), mounted to the microscope, and analyzed in ImageJ.

B. Device Design and Constraints

All particles must enter the device along the same flow-stream, if they are to experience identical electric field conditions for dielectrophoretic sorting; to do otherwise introduces confounding situations, such as certain particles eluding DEP

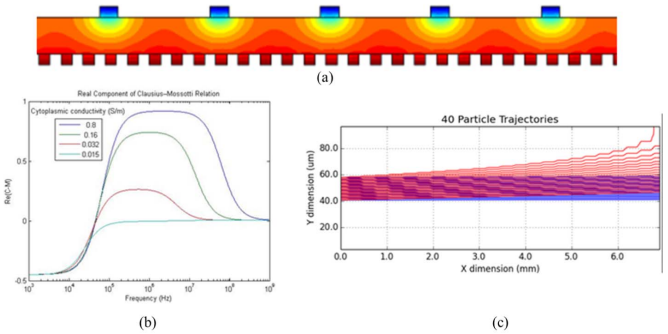

Fig. 2. (a) To predict particle trajectories, the device was drawn in COMSOL Multiphysics and a set of electric field and fluid field values was generated. These were imported into a custom Python program incorporating governing equations for laminar flow, particle collision, and DEP. (b) To predict the behavior of a specific particle type, the particle's dielectric properties were used to calculate a theoretical Clausius–Mossotti factor to be used in trajectory simulator. (c) Python script was used to calculate the trajectories of 40 particles, starting from 40 different positions across the width of the channel (Y dimension). The X dimension corresponds to the distance traveled along the DEP sorting region of the microfluidic device by each particle. In this simulation, particles entering at the 50-μm streamline or above in the Y dimension are deflected to a higher Y dimension (i.e., the left side of the microfluidic channel) as they traverse the length of the sorting region.

sorting completely by entering along a flowstream that only passes through weak field gradients. For this reason, the particle stream is focused into a tight band at the center of the main channel using a hydrodynamic focuser. Briefly, this is an established technology that takes advantage of the fact that under laminar flow conditions, such as those found in a microfluidic device, if multiple fluid streams converge into one, each will flow parallel to the others, with no convective mixing. The width percentage of each stream after convergence is proportional to its volumetric flow rate relative to the combined volumetric flow rate of all streams. In the presented device, particles are flowed into the main channel through a central inlet, while pure DEP buffer is flowed into the main channel through two side inlets. When the flow rate of pure DEP buffer into the main channel through these two side channels exceeds that of the particle suspension itself, the particle suspension is forced into a thin stream so narrow that particles enter the DEP sorting region approximately single-file [Fig. 2(c)].

Channel geometry was optimized by analyzing models built using COMSOL Multiphysics (COMSOL Inc., Los Angeles, CA) [Fig. 2(a)] and a custom Python package. The device was drawn in COMSOL and used to generate flow- and electric-field data. The data were exported and imported to a Python program in which governing equations for collision detection, fluid flow, and DEP were incorporated. Subsequently, simulated particles of various sizes and dielectric constants were flowed into the virtual device and particle trajectories were recorded. The geometries of the pickets and the focuser, as well as the voltage and frequency of the applied electronic signal, were adjusted until separation was achievable for various types and mixtures of particles.

Unlike vertical electrode fabrication using electroplating, fabrication using the solder alloy material imposed additional constraints on the optimal electrode design. The models showed that the electric field gradient was maximized in designs where the difference in size of electrodes on either side of the channel was greatest; however, the maximum usable electrode size was ultimately constrained by the upper limit on the radius of curvature, which would retain solder in the solder channel by surface tension.

In practice, electrode fabrication was most robust when the gaps between pickets were 50 μm or lower. This limitation could potentially be improved by decreasing the channel height (thus decreasing the radius of curvature in the perpendicular direction and increasing the overall surface tension at this location), however, our design required a channel height of 50 μm in order to prevent cell clogging and ensure a long device lifetime. The maximum gap between pickets for channels of different heights could be calculated by manipulation of the Young–Laplace equation

$$\Delta p = \gamma \left(\frac{1}{r_g} + \frac{1}{r_h} \right) \tag{5}$$

where r_g and r_h are the radius of curvatures dictated by the distance between pickets and the radius of curvature dictated by the channel height, respectively. In our system, the distance between pickets and the channel height are both 50 μm ($r_g = r_h = 25$ μm). Therefore, to determine the maximum gap between pickets that could be achieved by reducing the channel height to 30 μm, we manipulate the Young–Laplace equation to give the equivalent pressure

$$\Delta p = \gamma \left(\frac{1}{25} + \frac{1}{25} \right) = \gamma \left(\frac{1}{r_g} + \frac{1}{15} \right)$$
$$r_g = 75 \ \mu\text{m}. \tag{6}$$

The equations above can be employed in the design of channels for systems that can accommodate a microfluidic channel with a height smaller than 50 μm, in order to maximize the gradient of the electric field in the device, and thus the dielectrophoretic force that would develop.

IV. Results and Discussion

A. Cell Sorting

Freshly detached HeLa cells in PBS were separated into two aliquots at a concentration of 1E6/ml each. The cells were fluorescently stained with Carboxyfluorescein succinimidyl ester (CFSE) or propidium iodide (PI) to indicate viable and nonviable cells, respectively. Although treating the cells with a dye solution has the potential to alter their polarizability, a body of published work demonstrates the ability of electrodes in such a configuration to achieve dielectrophoretic cell separation in the absence of such dyes [11], [12].

One batch was stained with CFSE (Sigma-Aldrich, St. Louis, MO) at 50 μm for 30 min at room temperature; in live cells, CFSE is activated to fluorescent green at an excitation wavelength 488 nm, whereas in dead cells, no fluorescence occurs. The other batch was heat-killed via immersion in a 57 °C bath for 30 min [23]. Subsequently, these cells were stained with PI at 1% (wt/vol). In live cells, PI is unable to penetrate the cell membrane and no staining results, but dead cells' membranes are porated, granting the dye entry. Upon binding to the dead cells' exposed nucleic acids, PI fluoresces under an excitation wavelength of 561 nm [13].

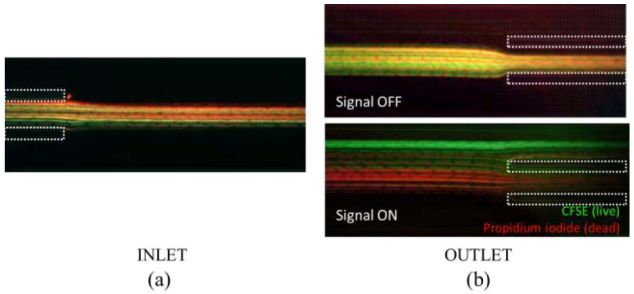

Fig. 3. Mixed population of live and dead cells are introduced to the device inlet, and separate into streams containing primarily live and dead cells at the outlet with the application of DEP force. Live cells were stained with CFSE dye (green) and dead cells were stained with propidium iodide (red). Images of particle traces from a video were stacked to show the trajectories of many particles. (a) At the inlet of the device, all of the cells (both live and dead) are focused in the middle of the three channels by hydrodynamic flow focusing. With no applied electric field, all cells, both live and dead, exit through the center outlet. (b) However, at 1 MHz and 50 V_{pp}, live cells, with their conductive cytosols and intact membranes, can form strong dipoles compared with those of the suspending media and experience pDEP, deflecting toward the upper edge of the flow channel and exiting through the upper outlet, indicated by the stream of green cells in the top channel. Dead cells experience no net DEP force and continue to exit the device through the center outlet, indicated by the stream of red cells in the middle channel. Note that while some cells stained with green exit through the middle channel with the dead cells, very few dead cells are incorrectly sorted into the upper outlet. Whitedashed outlines indicate the location of PDMS pilla.

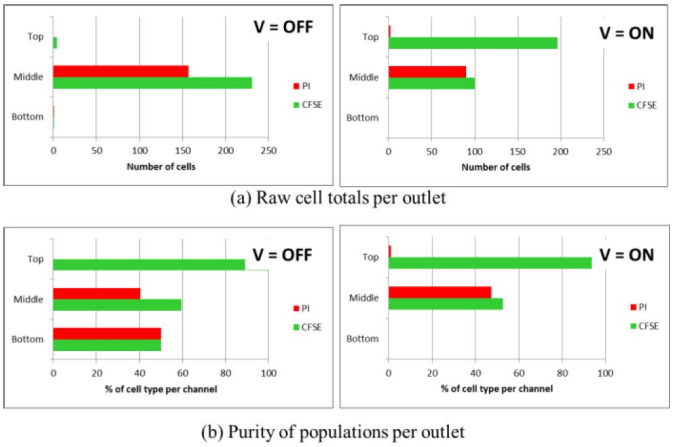

Fig. 4. Quantification of separation. Particle distribution across the channel width is measured using video footage as they exit the device through one of three outlets. (a) Separation is quantified in terms of the raw number of cells stained with CFSE or PI at each outlet with the voltage OFF (left) and ON (right). The results of separation of 507 cells are shown. (b) Purity of cell populations collected at each outlet with the voltage OFF (left) and ON (right).

Finally, both aliquots are recombined at a 1:1 ratio in a low-conductivity DEP buffer consisting of 8.5% sucrose (wt/vol), 0.3% dextrose (wt/vol), and 0.725% Roswell Park Memorial Institute (vol/vol); final conductivity and pH are 100 μS/cm and 7.38, respectively. Low-conductivity buffer is used to enable sorting of biological cells using positive DEP, as shown previously [7], [13], [24]. The final concentration of each cell type is 1E6/ml.

The basis of our separation of live and dead cells is the change in cytoplasmic conductivity that occurs as cells die and their membranes become permeable, allowing the cytoplasmic conductivity value to approach that of the media. As shown in the Clausius-Mossotti (CM) factor plot for our system (Fig. 2), the high conductivity of the cytoplasm in live cells (relative to the media's conductivity) results in a CM factor that is positive over several orders of magnitude in frequency. This results in a positive DEP force on these cells. As cells die and their cytoplasmic contents equilibrate with the cell media, the cytoplasmic conductivity drops and the CM factor becomes nearly zero or slightly negative, corresponding to zero or negative DEP force on these cells. Thus, separation of live cells by positive DEP force is enabled by lowering the medium conductivity to 100 μS/cm, which allows cells to experience a positive or negative DEP depending on the frequency of actuation used. Since the low conductivity buffer is osmotically balanced with the cells, it allows cells to maintain viability to accomplish this separation technique [25].

The prepared cell suspension was flowed into the device through the central inlet at a rate of 0.8 μL/min, while DEP buffer was flowed through the hydrodynamic focuser at 2.6 μL/min. In the deactivated device, all particles flow through the device without experiencing any lateral deflection and exit through the center outlet. When the device is activated at 1 MHz and 40 V_{pp}, however, live cells are deflected toward the top edge of the device and are sorted into the upper outlet, while dead cells experience no net dielectrophoretic force and exit through the center outlet [Fig. 3(b)]. To quantify sorting efficacy, particles exiting each channel were tallied for both the activated and deactivated devices, and the results were compared (Fig. 4).

The frequency and actuation used are similar to the optimal frequency and actuation parameters for a similar, previously published system [13]. A frequency of 1 MHz produces a positive DEP force in cells with intact membranes (i.e., high-cytoplasmic conductivity relative to the media conductivity), but produces a small negative DEP force in cells with compromised membranes (i.e., when the media and cytoplasmic conductivity are nearly equal). The actuation voltage of 40 V_{pp} was chosen as it provides a consistent deflection of live cells at the desired flow rates. A higher actuation voltage could potentially deflect the live cells more strongly, but would begin to have deleterious effects on the cell health and viability.

As shown, with the application of DEP force, the top outlet contained a significantly enriched population of cells stained with CFSE (98.9%). Despite the high purity of this stream, the data show that a significant population of cells staining with CFSE was not sorted to the top outlet. Due to the limitations of our imaging system, data were collected from the red and green fluorescence channels separately and at different time points, which prevented observation of cells that were co-stained with both CFSE and PI. It is likely that some of the CFSE-stained cells observed exiting the middle outlet of our device were in the early stages of death, as the CFSE stain may still be positive even when the cell membrane is compromised. With the ability to simultaneously image both the green and red fluorescence channels, the cells could have been identified as co-staining and thus be identified as dead (or dying) cells.

Despite these limitations, we have demonstrated a DEP sorting device that enables the separation of live cells from a mixture of live and dead cells with high purity. In addition, the device is capable of performing continuous (rather than batch)

separation of cells, which decreases the need for automation and may enable sorting of cells at a higher throughput than with batch separation procedures. Finally, the integration of the device with the established technology of a PCB will enable facile integration of electronic components, such as a signal generator, amplifier, and fluidic valves onto a completely integrated platform in future iterations of the device, realizing a true lab-on-a-chip with a small footprint.

V. Conclusion

The device presented addresses various obstacles in DEP cell sorting. Most importantly, vertically uniform electrical fields are generated by vertical electrodes, enabling continuous separation of cells and particles by balancing DEP force with fluid flow to steer different populations of cells or particles to different outlets. A prefocusing region in the device ensures that particles and cells enter the separation zone in single file, and thus experience an identical DEP force.

Additionally, the device is unique in its ability to integrate seamlessly with existing electronic components. Microfluidic cell sorters have experienced significant developments in the past decade, but there has been limited interest in the actual integration of these new technologies into real-world devices for portable point-of-care diagnostics. Importantly, the vertical electrodes can be fabricated quickly and out of the cleanroom, while the PCB substrate enables inexpensive and readily available substrates to produce these devices. By building this device on a standardized electronics platform, it is a significantly simpler task to integrate miniaturized external components such as pumps, valves, and switches, as well as electrical components such as an amplifier and a signal generator toward the development of a true lab-on-chip.

Acknowledgment

The authors would like to thank S. Vuong and R. Smith for preparing device graphics as well as for performing the simulation work in Python and COMSOL Multiphysics. The authors would also like to thank R. Chang for assistance with fabrication and T. Westerhof and J. Tucker for assistance with biological assays.

References

[1] D. R. Gossett *et al.*, "Label-free cell separation and sorting in microfluidic systems," *Anal. Bioanal. Chem.*, vol. 397, no. 8, pp. 3249–3267, 2010.
[2] E. Sollier *et al.*, "Size-selective collection of circulating tumor cells using Vortex technology," *Lab Chip*, vol. 14, no. 1, pp. 63–77, 2014.
[3] J. L. Nourse *et al.*, "Membrane biophysics define neuron and astrocyte progenitors in the neural lineage," *Stem Cells*, vol. 32, pp. 706–716, Mar. 2014.
[4] J. L. Prieto, J. Lu, J. L. Nourse, L. A. Flanagan, and A. P. Lee, "Frequency discretization in dielectrophoretic assisted cell sorting arrays to isolate neural cells," *Lab Chip*, vol. 12, no. 12, pp. 2182–2189, 2012.
[5] F. F. Becker, X.-B. Wang, Y. Huang, R. Pethig, J. Vykoukal, and P. R. C. Gascoyne, "The removal of human leukaemia cells from blood using interdigitated microelectrodes," *J. Phys. D, Appl. Phys.*, vol. 27, no. 12, p. 2659, 1994.
[6] F. F. Becker, X.-B. Wang, Y. Huang, R. Pethig, J. Vykoukal, and P. R. C. Gascoyne, "Separation of human breast cancer cells from blood by differential dielectric affinity," *Proc. Nat. Acad. Sci. USA*, vol. 92, no. 3, pp. 860–864, 1995.
[7] M. G. Simon *et al.*, "Increasing label-free stem cell sorting capacity to reach transplantation-scale throughput," *Biomicrofluidics*, vol. 8, no. 6, p. 064106, 2014.
[8] V. Gupta *et al.*, "ApoStream, a new dielectrophoretic device for antibody independent isolation and recovery of viable cancer cells from blood," *Biomicrofluidics*, vol. 6, no. 2, p. 024133, 2012.
[9] M. Muratore, V. Srsen, M. Waterfall, A. Downes, and R. Pethig, "Biomarker-free dielectrophoretic sorting of differentiating myoblast multipotent progenitor cells and their membrane analysis by Raman spectroscopy," *Biomicrofluidics*, vol. 6, no. 3, p. 034113, 2012.
[10] L. Wang, L. Flanagan, and A. P. Lee, "Side-wall vertical electrodes for lateral field microfluidic applications," *J. Microelectromech. Syst.*, vol. 16, no. 2, pp. 454–461, Apr. 2007.
[11] T. Braschler, N. Demierre, E. Nascimento, T. Silva, A. G. Oliva, and P. Renaud, "Continuous separation of cells by balanced dielectrophoretic forces at multiple frequencies," *Lab Chip*, vol. 8, no. 2, pp. 280–286, 2008.
[12] L. Wang, J. Lu, S. A. Marchenko, E. S. Monuki, L. A. Flanagan, and A. P. Lee, "Dual frequency dielectrophoresis with interdigitated sidewall electrodes for microfluidic flow-through separation of beads and cells," *Electrophoresis*, vol. 30, no. 5, pp. 782–791, 2009.
[13] J. Luo, E. L. Nelson, G. P. Li, and M. Bachman, "Microfluidic dielectrophoretic sorter using gel vertical electrodes," *Biomicrofluidics*, vol. 8, no. 3, p. 034105, 2014.
[14] N. Demierre, T. Braschler, P. Linderholm, U. Seger, H. van Lintel, and P. Renaud, "Characterization and optimization of liquid electrodes for lateral dielectrophoresis," *Lab Chip*, vol. 7, no. 3, pp. 355–365, 2007.
[15] B. H. Lapizco-Encinas, B. A. Simmons, E. B. Cummings, and Y. Fintschenko, "Dielectrophoretic concentration and separation of live and dead bacteria in an array of insulators," *Anal. Chem.*, vol. 76, no. 6, pp. 1571–1579, 2004.
[16] H. Shafiee, M. B. Sano, E. A. Henslee, J. L. Caldwell, and R. V. Davalos, "Selective isolation of live/dead cells using contactless dielectrophoresis (cDEP)," *Lab Chip*, vol. 10, no. 4, pp. 438–445, 2010.
[17] T. W. Herling, T. Müller, L. Rajah, J. N. Skepper, M. Vendruscolo, and T. P. J. Knowles, "Integration and characterization of solid wall electrodes in microfluidic devices fabricated in a single photolithography step," *Appl. Phys. Lett.*, vol. 102, no. 18, p. 184102, 2013.
[18] L. Altomare *et al.*, "Levitation and movement of human tumor cells using a printed circuit board device based on software-controlled dielectrophoresis," *Biotechnol. Bioeng.*, vol. 82, no. 4, pp. 474–479, 2003.
[19] L. A. Marshall, L. L. Wu, S. Babikian, M. Bachman, and J. G. Santiago, "Integrated printed circuit board device for cell lysis and nucleic acid extraction," *Anal. Chem.*, vol. 84, no. 21, pp. 9640–9645, 2012.
[20] R. Pethig, "Review article—Dielectrophoresis: Status of the theory, technology, and applications," *Biomicrofluidics*, vol. 4, no. 2, p. 022811, 2010.
[21] B. G. Hawkins, J. P. Gleghorn, and B. J. Kirby, *Methods in Bioengineering: Biomicrofabrication and Biomicrofluidics*, J. D. Zahn, Ed. Norwood, MA, USA: Artech House, 2009.
[22] H. Morgan and N. G. Green, *AC Electrokinetics: Colloids and Nanoparticles*. Baldock, U.K.: Research Studies Press Ltd., 2003.
[23] E. W. M. Kemna, L. I. Segerink, F. Wolbers, I. Vermes, and A. van den Berg, "Label-free, high-throughput, electrical detection of cells in droplets," *Analyst*, vol. 138, no. 16, pp. 4585–4592, 2013.
[24] L. A. Flanagan *et al.*, "Unique dielectric properties distinguish stem cells and their differentiated progeny," *Stem Cells*, vol. 26, pp. 656–665, Mar. 2008.
[25] J. Lu, C. A. Barrios, A. R. Dickson, J. L. Nourse, A. P. Lee, and L. A. Flanagan, "Advancing practical usage of microtechnology: A study of the functional consequences of dielectrophoresis on neural stem cells," *Integr. Biol.*, vol. 4, no. 10, pp. 1223–1236, 2012.

Jason Luo, photograph and biography not available at the time of publication.

Melinda G. Simon, photograph and biography not available at the time of publication.

Alan Y. L. Jiang, photograph and biography not available at the time of publication.

Edward L. Nelson, photograph and biography not available at the time of publication.

Abraham P. Lee, photograph and biography not available at the time of publication.

Guann-Pyng Li, photograph and biography not available at the time of publication.

Mark Bachman, photograph and biography not available at the time of publication.